Photoelectrochemical Study of Nitrogen-Doped Titanium Dioxide for Water Oxidation

Gemma Romualdo Torres,[†] Torbjörn Lindgren,[‡] Jun Lu,[‡] Claes-Göran Granqvist,[‡] and Sten-Eric Lindquist*[,†]

Department of Physical Chemistry, Uppsala University, P.O. Box 579, SE-751 23 Uppsala, Sweden, and Department of Engineering Sciences, The Ångström Laboratory, Uppsala University, P.O. Box 534, SE-751 21 Uppsala, Sweden

Received: November 14, 2003; In Final Form: February 10, 2004

This paper describes the photoelectrochemical response in aqueous electrolyte of nitrogen-doped titanium dioxide, $TiO_{2-x}N_x$. Thin film electrodes were prepared by reactive DC magnetron sputtering in an environment of Ar, O_2, and N_2. A typical film thickness was 0.85 μm. The crystal structure of the photoelectrochemically active films was mainly of rutile character, and scanning and transmission electron microscopy showed a highly porous parallel penniform nanostructure. It was conclusively shown that dioxygen could be generated from water by illumination of the $TiO_{2-x}N_x$ electrodes at moderate anodic potentials. The current density under 1000 W m^{-2} visible light from a sulfur lamp was 0.2 mA cm^{-2} at 0.55 V vs Ag/AgCl. Current−voltage characteristics under illumination were strongly dependent on the scan direction. Scanning the electrode from cathodic toward anodic potentials gave an onset potential similar to that of normal rutile TiO_2, whereas a reversed scan gave an onset of photocurrent (depending on the light source) anodically upshifted by up to 0.8 V from its normal position. Moreover, a cathodic current was observed during the latter scans. This current was induced by the illumination at anodic potentials. This nonfaradic current was ascribed to photoinduced electron trap states distributed in an approximately 1.3 V wide range negative of the conduction band (CB) edge. These states also were active as electron−hole recombination centers. The density of this new set of states was $\sim 2 \times 10^{20}$ cm^{-3}, i.e., similar to the density of nitrogen atoms. They can be activated by light, even at wavelengths beyond 700 nm, and work as long-lived electron traps; hence, they have properties that are different from those of the earlier found Ti^{3+} (3*d*) states, also located below the CB of TiO_2. The new states occur as a consequence of the nitrogen doping, but is not necessarily an intrinsic property of pure $TiO_{2-x}N_x$. Recombination via the new states—in conjunction with slow hole transport in the nitrogen-created band above the valence band edge—was suggested to be the cause of the large anodic shift of the onset potential for cathodic scans and of the moderate water oxidation efficiency of the $TiO_{2-x}N_x$ thin film electrodes.

I. Introduction

Direct splitting of water into dihydrogen (H_2) and dioxygen (O_2) by solar light in photoelectrochemical cells has received much attention, since hydrogen is often considered the fuel of the future.[1] Honda and Fujishima[2] were the first to report successful photoelectrochemical splitting of water. They used a semiconductor electrode based on rutile titanium dioxide, TiO_2. Since then, both rutile and anatase crystal forms of TiO_2 have been extensively studied for photoelectrochemical and photocatalytic applications owing to their photoactivity, high corrosion resistance, and nonhazardous nature.[3−5]

However there are disadvantages with TiO_2, a major one with regard to solar energy applications being that the band gap energies, 3.0 eV for rutile and 3.2 eV for anatase, only allow ultraviolet (UV) absorption. To improve the photoelectrochemical efficiency of the material, it is desirable to red-shift the photoelectrochemical onset in order to also include the less energetic but more intense visible part of the solar spectrum. Traditionally this has been achieved by anchoring organic dyes to the surface, and this approach has been successful in dye-sensitized solar cells.[6] However, the commonly used ruthenium-based organic dyes are expensive, and moreover, the long-term stability of many dyes can be questioned. Another problem with organic dyes is that they can detach from the surface when employed in aqueous solution. Therefore there is a need to increase the photoelectrochemically active spectrum by other approaches.

Already in 1986, Sato[7] reported about photocatalytic activity in visible light for TiO_2 prepared and calcinated with NH_4OH. However it took almost fifteen years from then until nitrogen-doped TiO_2 again was considered for photocatalytic applications. Iin 2001, Taga et al.[8,9] reported that nitrogen-doped TiO_2 (denoted $TiO_{2-x}N_x$) shows a narrower band gap and better photocatalytic activity under visible light than the corresponding undoped TiO_2. With this approach in mind, we recently synthesized nitrogen-doped TiO_2 films by means of reactive DC magnetron sputtering.[10,11] The photoelectrochemical and optical properties showed that the new band-gap states created by doping indeed improved the photoresponse in the visible region.

It is presently generally accepted that visible light absorption in nitrogen-doped TiO_2 is due to substitution of oxygen by nitrogen, which results in a mix of N2*p* and O2*p* states.[8,12] The nitrogen-generated states lie energetically above the O2*p* valence band of TiO_2, as was shown experimentally by Lindgren et al.,[10] who measured the open-circuit potential under irradiation of dye-incorporated samples. Similar experimental evidence was

* Corresponding author. E-mail: sten@fki.uu.se.
[†] Department of Physical Chemistry.
[‡] Department of Engineering Sciences, The Ångström Laboratory.

10.1021/jp037477s CCC: $27.50 © 2004 American Chemical Society
Published on Web 04/20/2004

found by Sakthivel and Kisch.[11] Accordingly, the conduction band edge should remain unchanged by nitrogen doping, and the expected needed bias should be low when $TiO_{2-x}N_x$ is used as an electrode for water oxidation. Such a material would be of great interest for direct water splitting in a photoelectrochemical cell or for use in a tandem cell such as the one described by Grätzel.[12]

Recently, efficient photoelectrochemical response in aqueous electrolyte has been reported for other materials that can be described as anion-doped TiO_2. Specifically, carbon-modified TiO_2,[13] sulfur-doped TiO_2,[14,15] and $TiN_xO_yF_z$[16] are novel and interesting materials which have shown good photocatalytic response in visible light.

The present paper supplements our previous studies of sputter-deposited nitrogen-doped TiO_2 films[10,11] by reporting on the photoelectrochemical behavior of such electrodes in aqueous electrolyte.

II. Experimental Section

Electrodes and Electrolytes. Thin films were prepared according to a general thin-film sputtering method described by Rodriguez et al.[17] The same sputter parameters were used as in work by Gómez et al.,[18] though with a current of 0.75 A and an addition of nitrogen in the deposition chamber.[10,19] One of the crucial sputter parameters for the elaboration of the films is the nitrogen gas flow ratio, defined as $\Phi = f(N_2)/f$, where $f = f(O_2) + f(Ar) + f(N_2)$. Our previous results[10,11] showed that optimum performance occurred at $\Phi = 0.0063$, and the present study is focused on $TiO_{2-x}N_x$ films made under this condition. For convenience, films prepared with nitrogen will be called nitrogen-doped TiO_2, or $TiO_{2-x}N_x$, and films prepared without nitrogen will be called undoped TiO_2 (the authors are aware that also the latter films can be doped, for instance by oxygen vacancies, and that the fraction of nitrogen, vide infra, is well above typical doping levels of semiconductors). The film thickness, determined by surface profilometry using a Tencor AlphaStep instrument, was 0.85 ± 0.05 μm for all films. The nitrogen-doped electrodes were bright yellow, transparent, and slightly light scattering. They were chemically, mechanically, and thermally stable under the experimental conditions used. As a quick stability test, a film of nitrogen-doped rutile TiO_2 was annealed in an open atmosphere at 500 °C for 1 h without any change in the optical or photoelectrochemical properties. No long-term photoelectrochemical stability tests were performed, but repeated photoelectrochemical studies on the same nitrogen-doped electrode during one full year did not lead to any evidence for degradation. Asahi et al.[8] reported for their $TiO_{2-x}N_x$ sample that they resisted the attack of acids and alkaline solvents such as H_2SO_4, HCl, and NaOH at ambient temperature. Their photocatalytic performance was stable during successive use under 100 W mercury lamp irradiation for more than 3 months.

The films were deposited onto soda lime glass substrates (standard microscope slides) for optical characterization and onto electrically conductive glass for photoelectrochemical studies. The conducting glass substrates had a coating of fluorine-doped SnO_2 with a sheet resistance of 8Ω/□ (Tec8, Hartford Glass Company, Inc.). Electrical contacts were established by fixing copper wires to the conducting layer on the glass substrate by use of conductive silver paint. Exposed areas of the back contact and edges were carefully sealed with epoxy resin. The working electrode area was about 0.5 cm^2 for each sample.

Reagent-grade chemicals and Milli-Q water (Millipore Corp.) were used in the electrolyte preparation. The electrolyte was 0.1 M NaOH (pH 13) if not otherwise stated. The effect of pH was studied by use of different phosphate buffers.

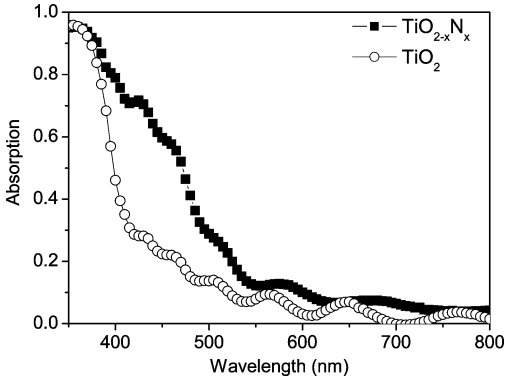

Figure 1. Spectral absorption for films sputtered with and without an addition of nitrogen during deposition. The nitrogen-doped film is denoted $TiO_{2-x}N_x$, and the undoped film is denoted TiO_2.

Characterization of the Films. Total spectral transmittance, T_λ, and reflectance, R_λ, were recorded using a Perkin-Elmer Lambda 900 spectrophotometer fitted with a 150-mm-diameter integrating sphere. Spectral absorption, A_λ, was obtained from

$$A_\lambda = 1 - T_\lambda - R_\lambda \quad (1)$$

Figure 1 shows data for undoped and nitrogen-doped TiO_2. The interference-like pattern probably originates from difficulties in measuring the total reflectance. It can be seen that the onset wavelength for absorption in $TiO_{2-x}N_x$ is located around 550 nm, i.e., shifted well into the visible region. For undoped TiO_2, on the other hand, the onset is closer to the ultraviolet region.

Transmission electron microscopy (TEM) was carried out using a field emission gun TECNAI F30 ST operated at 300 kV with a point resolution of 2.05 Å. The sample preparation for TEM followed the procedure described by Gómez et al. [20] Figure 2 depicts a cross-section of a $TiO_{2-x}N_x$ film. The TEM image illustrates a porous parallel penniform nanostructure, which is strikingly similar to the nanostructure of TiO_2 samples that were sputter-deposited under similar conditions—though without nitrogen addition—in previous work.[18,20,21]

Undoped TiO_2 films had rutile structure, and $TiO_{2-x}N_x$ films were mainly of rutile type though with some traces of anatase, as found in earlier work using X-ray diffraction[10] as well as from the electron diffractogram in Figure 2.

Elemental compositions of the films were studied by X-ray photoelectron spectroscopy. As reported in an earlier paper of ours,[11] about 0.65% of the oxygen sites were substituted by nitrogen, which corresponds to a composition equal to $TiO_{1.987}N_{0.013}$.

An electrochemical cell was used for three-electrode experiments. It was comprised of a closed vessel with an inside wall of black Teflon to avoid scattered and reflected light. The cell was equipped with quartz windows, and the design of the vessel permitted illumination of both sides of the sample: front side (light incident on the electrolyte/electrode interface, denoted EE) as well as backside (light incident on the substrate/electrode interface, denoted SE).[22] An Ag/AgCl electrode (SSE) in saturated KCl (Metrohm AG) was used as a reference electrode. According to the manufacturer's calibration, this reference electrode has a potential of +197 mV versus NHE at 25 °C. If not otherwise mentioned, all potentials in the present study are referred to the SSE at 25 °C. A platinum grid was used as a counter electrode. The reference and counter electrodes were enclosed in separate glass chambers with glass frits. The

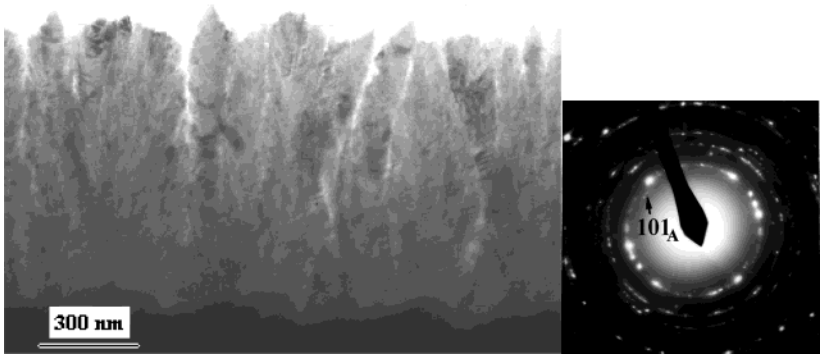

Figure 2. Transmission electron micrograph of a cross-section through a sputter-deposited $TiO_{2-x}N_x$ film (left), and electron diffractogram of the same film (right).

electrolyte was mechanically stirred and degassed by purging with 99.99% pure nitrogen gas before and during each experiment. All experiments were performed at 22 °C. The variation of the potential of the reference electrode at that temperature, compared to the case of 25 °C, was found negligible.

The experimental setup for incident photon-to-current efficiency (IPCE) measurements was similar to the one described before,[23] but using a Cermax Model LX 300 UV lamp (ILC Technology) and a computer-controlled 1/8 m monochromator (CM, 110) assisted by an automatic filter wheel (CM, AB301). The intensity was measured with an optical power meter (Newport, 1830-C). The light intensity was low, typically in the 1 mW/cm^2 range.

A xenon lamp and a sulfur plasma lamp were used separately during the photoelectrochemical measurements. A GG-3 cutoff filter was used to isolate the visible fraction in the xenon lamp ($\lambda > 400$ nm). Similarly, a UG-5 filter was used to isolate the UV fraction of this lamp ($\lambda < 400$ nm). According to the specification for the sulfur plasma lamp, the light intensity for wavelengths below 380 nm was less than 0.8% of the total output. The light intensity was measured by a pyranometer (Kipp & Zonen CM 11). The light intensity for the pure unfiltered xenon light was 1750 W/m^2. The corresponding filtered xenon light was 250 W/m^2 for the UV fraction (UG-5 filter) and 750 W/m^2 for the visible fraction (GG-3 filter). If not otherwise stated, the light intensity of the sulfur plasma light corresponded to 1000 W/m^2 (approximately 1 sun).

A computer-controlled potentiostat (Autolab μII, ECO Chemie BV) was used for (photo)electrochemical experiments, both in the dark and under illumination. The spectral incident photon-to-current efficiency was calculated according to

$$\mathrm{IPCE}_\lambda = \frac{hc}{q}\frac{I_{\mathrm{ph},\lambda}}{P_\lambda \lambda} \qquad (2)$$

where $I_{\mathrm{ph},\lambda}$ is the photocurrent, P_λ is the light power intensity, and h, c, and q have their usual meaning of Planck's constant, speed of light in a vacuum, and elementary charge, respectively. IPCE_λ plotted versus wavelength is called an action spectrum. The IPCE_λ measurements were carried out with irradiation through the SE interface as well as through the EE interface. In all action spectra recorded with SE illumination, corrections were made for absorption and reflection losses due to the conducting glass substrate. Since the transmission through the glass is less than 50% for $\lambda < 350$ nm and the photocurrents are low, this part of the corrected SE action spectrum contained relatively large errors and is therefore not shown. The absorbed photon-to-current efficiency, APCE_λ (also called the quantum yield) was obtained by dividing the IPCE_λ with the absorption.[10]

III. Results and Discussion

Electron Trapping and Recombination Shown by *j*−*V* Characteristics. Current density j vs voltage V was analyzed in 0.1 M NaOH in the dark and under illumination, using a scan rate of 5 mV s^{-1} and a light intensity of 300 W/m^2. During these experiments, the solution was purged with N_2. The sulfur plasma light was used, and the electrode was illuminated through the SE interface. Scans starting at an anodic potential and running toward negative potentials are called *cathodic* scans, and scans starting from cathodic potentials and going positive are called *anodic* scans.

Comparing the data for nitrogen-doped TiO_2 in Figures 3a and 3b, it can be seen that the photocurrent depends strongly on the scan direction. Dashed lines represent scans done with a chopper attached to the system, full lines refer to corresponding scans under illumination when no chopper was used and when scans were taken in the dark, and, finally, the filled circles show the response under photostationary conditions (meaning registration of a steady-state current during constant prolonged illumination). For the latter case, we did not observe any net anodic photocurrent at potentials below −0.5 V. It is apparent from Figure 3 that the agreement between the continuous and chopped scans is almost complete, the only difference being that the chopped light gives rise to clear photocurrent transients. These transients are particularly evident for the anodic scan (Figure 3a) in the interval from the onset potential, U_{on}, to about +0.1 V. The appearance of the photoinduced transients is indicative of severe recombination.

There is a remarkable change in U_{on} upon a shift of scan direction from −0.90 V to −0.13 V (cf. Figures 3a and 3b). For a perfect *n*-doped semiconductor with a reasonably high doping density and with no recombination centers, U_{on} should coincide with the flat-band potential and be positioned just below the conduction band (CB) edge.[24] From previous studies,[4] the expected onset of photocurrent for rutile TiO_2 at the pH of a 0.1 M NaOH solution should be located at approximately −0.8 V vs NHE, i.e., at −1.0 V. This is indeed close to the observed U_{on} for the anodic scan (cf. Figure 3a) but far from the experimentally observed U_{on} for the cathodic scan (cf. Figure 3b).

As can be expected, the onset of the *photostationary* anodic current shown in Figures 3a and 3b starts at a very low level around −0.5 V, i.e., between the onsets of photocurrent for the anodic ($U_{\mathrm{on}} = -0.9$ V) and the cathodic ($U_{\mathrm{on}} = -0.13$ V) scans. The interpretation of this substantial anodic shift again lies in severe recombination in the potential range from −0.9 V to at least +0.1 V. As will be seen further on, the distribution of states causing the recombination are present at potentials even up to approximately +0.4 V.

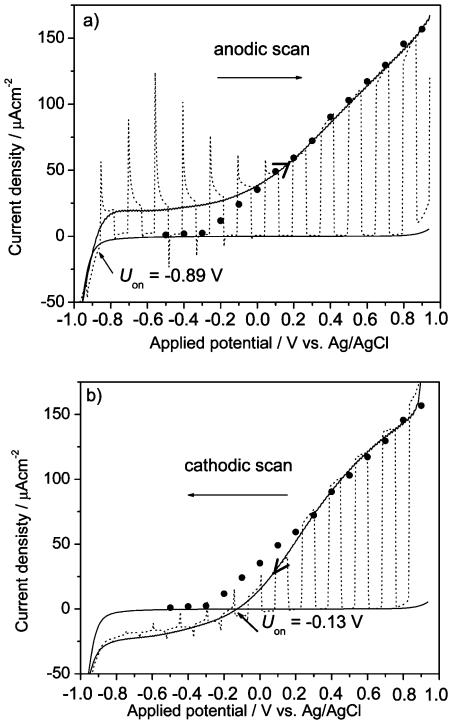

Figure 3. Current−voltage characteristics measured on a sputter-deposited $TiO_{2-x}N_x$ film. Parts (a) and (b) show the photoresponse in 0.1 M NaOH for scanning toward anodic potentials (*anodic* scan) and toward cathodic potentials (*cathodic* scan), respectively. Dashed lines represent scans done with a chopper attached to the system, full lines refer to corresponding scans under illumination when no chopper was used and scans were taken in the dark, and filled circles show the response under photostationary conditions. Detailed information for the variously indicated data are given in the main text. U_{on} signifies an onset potential. Illumination was from the substrate/electrolyte side, using a sulfur lamp with intensity close to 300 W/m^2. The scanning rate was 5 mV s^{-1}.

Cathodic Current Reminiscent of Illumination at Anodic Potentials. A remarkable observation is that cathodic scans give rise to cathodic currents negative of the U_{on} at −0.13 V (Figure 3b). This cathodic current is apparently induced by the illumination at anodic potentials. It should be noted in this context that scans performed in the dark do not vary with scan direction, and that the dark current is negligible in a broad range from −0.8 to +0.9 V (Figure 3). Above +0.90 V and below −0.90 V, the normal potential-induced oxidation and reduction of water is observed.

The detection of a cathodic net current induced by the illumination was followed up by a set of complementary experiments (data not shown). Thus the $TiO_{2-x}N_x$ thin film electrode, kept at an anodic potential (typically 0.6 V), was illuminated for a limited time (in the interval 5 to 60 min) by light from different light sources. The light sources were (*i*) the xenon lamp, (*ii*) the sulfur lamp, and the latter lamp furnished with (*iii*) OG2 or (*iv*) RG715 filters. The OG2 and RG715 filters have cutoffs only allowing light with $\lambda > 550$ nm and $\lambda > 715$ nm to be transmitted, respectively. Independent of light source, the cathodic scans always showed a cathodic net current in the range from about +0.4 V to −0.9 V, while no cathodic current was observed when the electrode was rested for a similar duration at the same potential in the dark. For light sources (*i*) and (*ii*), the cathodic current reached a saturation limit after a few minutes, while light sources (*iii*) and (*iv*) required longer times to reach that limit: typically 15 min for (*iii*) and 30 min for (*iv*).

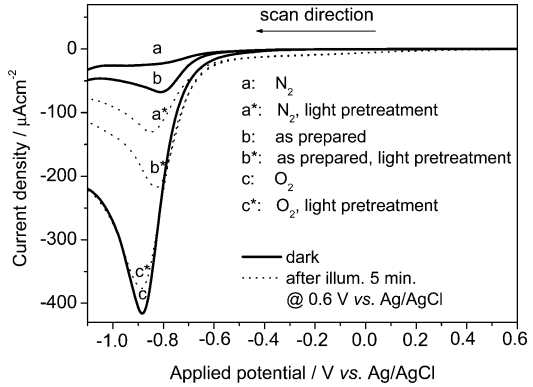

Figure 4. Current−voltage characteristics measured on a sputter-deposited $TiO_{2-x}N_x$ film. Data were first recorded in the dark with the film purged with N_2 (a), in equilibrium with air (b), and saturated with O_2 (c). Corresponding data, denoted with asterisks, were then recorded immediately after illumination with visible light for 5 min at an applied potential of +0.6 V. The scanning rate was 5 mV s^{-1}.

Long-Lived Photoinduced Electron Trapping States. Our conclusion from the experiments described above is that UV, visible, and infrared (IR) light ($\lambda > 715$ nm) empties states in the band gap—i.e., states that trap electrons during the cathodic scan. The fact that the onset of the cathodic current in N_2-purged solutions appears directly after the crossover point of the dark current at −0.13 V shows that these states, and not the reduction of O_2 (formed at more anodic potentials during illumination), are the electron acceptors. Therefore, the registered cathodic current is "capacitive" rather than faradic in character. Further evidence of the latter will be given in the following sections.

Thus we propose that the cathodic current observed in the potential regime below −0.13 V (Figure 3b) is due to the existence of photoinduced electron acceptors. Since these states are activated to work as long-lived electron traps by light (even at $\lambda > 715$ nm), they have different properties than those earlier found for TiO_2 Ti^{3+} (3*d*) states. They are also located below the CB. They can therefore *not* be identified with latter, but rather are a consequence of the nitrogen doping.

Apparently the new states also work as efficient recombination centers in the $TiO_{2-x}N_x$ film electrodes (cf. the transients in Figure 3a) and are the cause of the dramatic negative shift of U_{on} for cathodic scans (compare Figures 3a and 3b). They are also the cause of the anodic shift of the anodic photocurrent under photostationary conditions.

Confirmation of Oxygen Evolution, and Effects of Oxygen in the Solution. Photoelectrochemical O_2 evolution at the $TiO_{2-x}N_x$ electrode was proved by analyzing the $j-V$ characteristics in the dark upon variations of the concentration of O_2 in the solution. Thus a 0.1 M NaOH solution was used (*i*) as purged with N_2, (*ii*) as prepared in equilibrium with air, and (*iii*) as saturated with O_2. Results are shown in Figure 4. For each condition (*i*) to (*iii*), an $j-V$ curve was first recorded in the dark from +0.6 V to −1.1 V. Then the semiconductor was illuminated with visible light for 5 min at an applied potential of +0.6 V, and a second $j-V$ curve was immediately recorded in the dark. The solution was stirred when purged with N_2 gas or loaded with O_2, but the electrolyte was allowed to stabilize during the illumination and the recordings of the $j-V$ curves. This means that O_2, generated by photooxidation of water at the electrode surface, was not swept away by convection and therefore could be detected electrochemically.

When the solution was saturated with O_2 (corresponding to a dioxygen concentration, $[O_2]$, of ∼1.25 mM), an intense cathodic O_2 peak was observed around −0.85 V (curve c in

Figure 4). In the solution in equilibrium with air ($[O_2] \times 93$ 0.25 mM), the same peak decreased (curve b) in correspondence with the decrease in $[O_2]$. Finally, when the solution was purged with N_2, the peak disappeared more or less completely (curve a). After pretreatment of the electrode with light for 5 min at an applied potential of 0.6 V, a dioxygen peak appeared in the pre-purged solution (curve a*). Similarly, in the solution in equilibrium with air the O_2 the current peak increased considerably (curve b*), while the peak for an O_2-saturated solution rather decreased (curve c*). From the difference between curves a and a*, and b and b*, we immediately see that O_2 is formed under illumination with visible light. Since curves c and c* both represent experiments with O_2-saturated solutions, we would as a first approximation not expect any difference after illumination; however, we observed a *decrease* that will be explained below.

After illumination, curves a*, b*, and c* in Figure 4 all show a slight increase in cathodic current in the potential range from −0.4 V to + 0.4 V. This cathodic current is again due to the electron trapping states induced by the illumination at anodic potentials, in agreement with what was observed in Figure 3b below −0.13 V and discussed above.

If we assume that the electron trapping is faster than, or at least of the same rate as, the electron-transfer process causing the reduction of O_2 (the reaction most probably being $O_2 + e^- \rightarrow O_2^-$), the observed decrease in curve c* compared to curve c can be understood. Thus, if the solution remains saturated with respect to O_2 also after illumination, which is reasonable, the observed decrease is simply due to the fact that a fraction of the electrons are trapped in the $TiO_{2-x}N_x$ electrode and therefore not available for the faradic reduction process of O_2. In other words, the difference in the integrated charge under the current plots between curves c* and c, in the potential interval from −0.82 V to −0.98 V, is a reflection of the number of trapping states per unit area of electrode in this interval. Furthermore, since the recordings of the data in Figure 4 were performed either in the dark (curves a, b, and c), or in the dark after illumination (curves a*, b*, and c*), it can be seen that the distribution of the trapping states—reflected by the difference between the curves recorded in the dark and those recorded after illumination—extends from −0.4 V to approximately +0.4 V. Below about −0.4 V, trapping states in a* and b* coincide with the dioxygen peak**.** Their existence is, however, evident from purged solutions (cf. Figure 3b and also Figures 5 and 6, vide infra). The decrease in the anodic photocurrent in the range −0.13 V to +0.4 V in Figure 3b, compared to data in Figure 3a, provides further evidence of the photoinduced electron trap states, i.e., states which after electron trapping by capturing a hole work as recombination centers.

To further check on the generation of O_2 under visible light illumination, the experiments above were repeated with a thin Pt-wire electrode mounted in close proximity to the $TiO_{2-x}N_x$ electrode (data not shown). A reductive dioxygen peak was observed at −0.25 V. The dioxygen detection signal from the Pt-wire followed the same trend as when $TiO_{2-x}N_x$ was used for dioxygen detection. This proves conclusively that O_2 was evolved during the illumination of the $TiO_{2-x}N_x$ electrode.

Effect of Light Intensity. With the same experimental conditions as those described above in connection with Figure 3b, $j-V$ characteristics for *cathodic* scans were repeated at different light intensities from the sulfur lamp. As seen from Figure 5a, the photocurrent onset potential is independent of light intensity and remains located around −0.15 V. Positive of this U_{on}, the current increases with light intensity. Figure 5b shows the current density as a function of light intensity at a constant potential of 0.85 V. Up to 500 W/m^2, the photocurrent scales linearly with light intensity**.** At 1000 W m^{-2} (corresponding to one sun) visible light from the sulfur lamp, j is ∼0.23 mA**.** For higher light intensities, j deviates negatively from linearity. Such a behavior is generally explained by losses due to electron−hole recombination.[25,26]

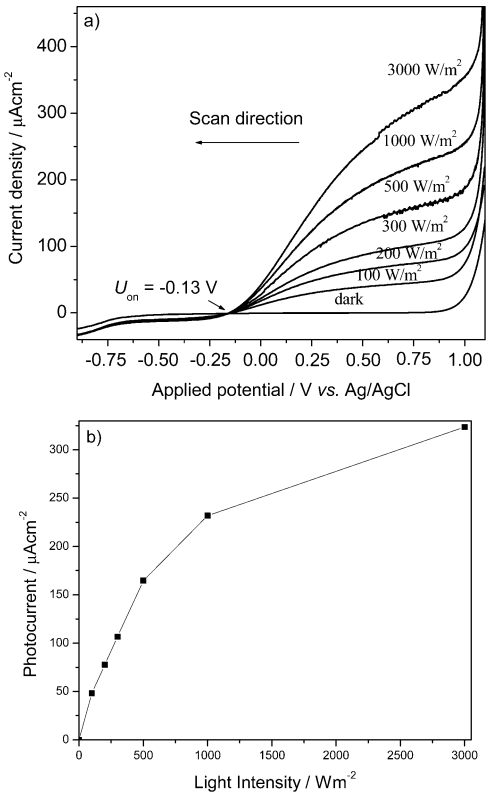

Figure 5. Current−voltage characteristics at different light intensities (a) and current vs light intensity at a voltage of 0.85 V (b) measured on a sputter-deposited $TiO_{2-x}N_x$ film. The electrode was illuminated from the substrate/electrolyte interface in a 0.1 M NaOH solution. U_{on} signifies an onset potential. The scanning rate was 5 mV s^{-1}.

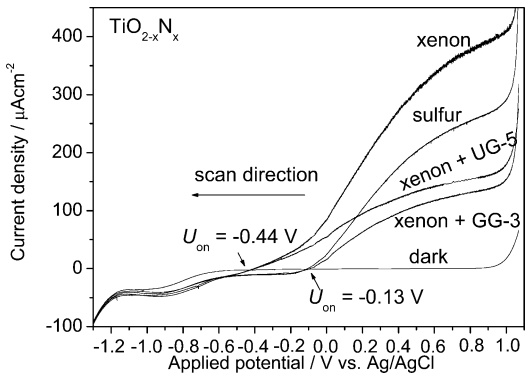

Figure 6. Current−voltage characteristics measured on a sputter-deposited $TiO_{2-x}N_x$ film under irradiation from different light sources, as elaborated in the main text. The electrode was illuminated from the substrate/electrolyte interface in a 0.1 M NaOH solution. U_{on} signifies an onset potential. The scanning rate was 5 mV s^{-1}.

The amplitude of the *cathodic current*—above interpreted as a "capacitive" current caused by electron trapping states induced by the illumination at anodic potentials—depends very weakly on light intensity in the regime 100 to 3000 W m^{-2}. This current depends neither on the concentration of electron scavengers, e.g., dissolved O_2, nor on purging with nitrogen, as shown in Figure 4. This implies that the cathodic current, photoinduced

at anodic potentials, is not due to photoconduction, which is reported to be dependent on light intensity incident on the electrode surface as well as on electron scavengers (such as O_2) for TiO_2 in aqueous solution.[27] Photoconduction can also be excluded on the basis that no net cathodic photocurrents are seen below U_{on} for chopped light; cf. the dashed curve in Figure 3b. This further strengthens the argument for interpreting the cathodic current below −0.13 V—observed only after illumination at anodic potentials in Figures 3b and 5, and observed in the potential range −0.4 V to +0.4 V in Figure 4—as being due to electron trapping states.

Origin of the Cathodic Current Induced by Illumination. Summing up, data in Figures 3, 4, and 5 show that the cathodic current is registered after illumination at anodic potentials in a wide range: from approximately −0.9 V to +0.4 V. This net "capacitive" cathodic current reflects the range over which the electron trapping states are distributed. Thus, the states are found in an interval lying ∼1.3 V from the conduction band and downward. The fact that these states can be excited by IR light strengthens the evidence that they are located in this range. Excitation from a state at an energetic position of ∼1.3 eV can indeed take place to the conduction band by light with $\lambda > 730$ nm (corresponding to an energy of 1.73 eV). The result is indicative of the existence of an absorption band in the IR region. The extinction coefficient of this band is probably very weak and it will be further weakened by illumination. We have so far not been able to observe the band spectroscopically.

The fact that the cathodic current below U_{on} in Figure 5 saturates at 100 W/m^2 of visible light shows that *all* traps are filled already at that intensity. The total charge that can be collected in the states per projected surface unit of electrode, Q, can therefore be estimated by integrating cathodic time−current curves below the dark−current curve in this interval. Using a scan rate of 5 mV s^{-1} and data from Figure 4 in the interval +0.4 V to −0.25 V as well as data from Figure 3b in the interval −0.25 V to − 1.0 V, a rough estimate gives $Q \times 93$ 3×10^{-3} A s cm^{-2}. Assuming that the states are homogeneously distributed in the electrode material and using a film thickness t of 850 nm, this corresponds to a density of electron trapping states equal to $N_{D,t} = Q/q \times 93\ 2 \times 10^{20}$cm^{-3}**.** We can compare this density with the number of nitrogen atoms per unit volume in the electrode material. The fraction x of nitrogen in $TiO_{2-x}N_x$ was determined to be 0.65%, as mentioned in the Experimental Section above. Assuming a porosity p of 50%, and a molecular weight ($M = 79.9$ g mol^{-1}) as well as a density ($\rho = 4.26$ g cm^{-3}) of $TiO_{2-x}N_x$ to be the same as for rutile TiO_2, then the estimated number of nitrogen atoms per unit volume in $TiO_{2-x}N_x$ is obtained from $N_{D,N} = xp\rho N_A/M = 1 \times 10^{20}$cm^{-3}, where N_A is Avogadro's number. Hence $N_{D,N}$ is of the same order of magnitude as $N_{D,t}$. Considering the uncertainty in the estimated values, the agreement is good enough to propose that the electron trapping states are linked to the presence of substitutional nitrogen atoms in the lattice of $TiO_{2-x}N_x$. The material is nanoporous, and therefore we cannot conclusively judge whether the states are located in the bulk, at the surface, or both.

Thus, in addition to the set of states distributed in a range just above and around the valence band (VB) of $TiO_{2-x}N_x$, described in an earlier paper of ours,[10] there is now evidence of a corresponding set of states caused by the nitrogen doping in a range ∼1.3 eV below the CB. While the former give rise to absorption of photons and photocurrents in the visible range up to 550 nm in wavelength,[10] the latter are efficient electron traps and sites for electron−hole recombination after illumination at anodic potentials.

Effects of UV and/or Visible Light Illumination. As mentioned above, the independence on light intensity and electron acceptors in the electrolyte indicates that the cathodic current induced by illumination at anodic potentials is due to internal properties of the electrode material. We interpreted the cathodic current as due to electron trap states in an interval from +0.4 to −0.9 V. To further study the nature of these states and the charge transport in $TiO_{2-x}N_x$, the cathodic $j-V$ scans were repeated using four separate light sources with different spectral distributions. The result of this study is shown in Figure 6.

As shown in the present work and earlier,[28] the apparent U_{on} of the photocurrent for $TiO_{2-x}N_x$ was around −0.15 V when cathodic scans were applied and visible light from the sulfur lamp was used. Now we also employed a xenon lamp furnished with a GG-3 cutoff filter to eliminate the UV fraction of the irradiation. As expected, the position of U_{on} remained the same as for the sulfur lamp. When we used an unfiltered xenon lamp, or a xenon lamp furnished with a UG-5 filter (having a band-pass filter for UV and thus removing visible light above 400 nm), U_{on} was substantially shifted cathodically to approximately −0.44 V. The cathodic current below U_{on}, induced by illumination at anodic potentials, was still observed no matter what light source was used.

The striking observation in Figure 6 is that U_{on} is located at more anodic potentials for the light sources giving only visible light than for those containing UV light. Apparently, UV light gives a higher probability for the electrons and holes to leave the electrode and contribute to a faradic photocurrent and oxidizing water. As shown in previous papers,[8,10,11,29] substituting nitrogen for oxygen in TiO_2 introduces states in regime around and above the valence band. The shift of the spectral response into the visible region was ascribed to this set of states, centered on a maximum located ∼2.9 eV below the lower edge of the conduction band.[10]

While the UV light is able to create holes in the VB and promote electrons to the CB, visible light allows a promotion of electrons to CB only by transitions from the set of states just above the VB, created by nitrogen doping. Thus the conditions for transport of electrons in the CB are the same in both cases, but the conditions for hole transport may differ dramatically. It is reasonable to believe that the mobility of holes in the VB is much higher than for the hole transport between (probably localized) states created by the nitrogen doping. Thus the shift of U_{on} due to a change from visible to UV illumination in Figure 6 may be explained by considering this difference in mobility of holes. In other words, the rate of hole transfer to create a faradic photooxidation current is faster in the case of VB holes. This implies that the probability for electrons from the CB that are trapped to recombine with holes is smaller, and the faradic net photooxidation current prevails at even lower potentials. However, we must also consider that the driving force for oxidation of water is higher for the CB holes than for holes in the states around and above the VB created by the nitrogen doping. A schematic picture of the energetics and processes in the $TiO_{2-x}N_x$ thin film photoanode is given in Figure 7.

Summing up our results and the discussion of the present section, we can state that the hole transport in $TiO_{2-x}N_x$ and/or the hole transfer in the subsequent oxidation of water may be limiting steps reducing the efficiency of the $TiO_{2-x}N_x$ photoanode for water oxidation in the visible region. Of these two

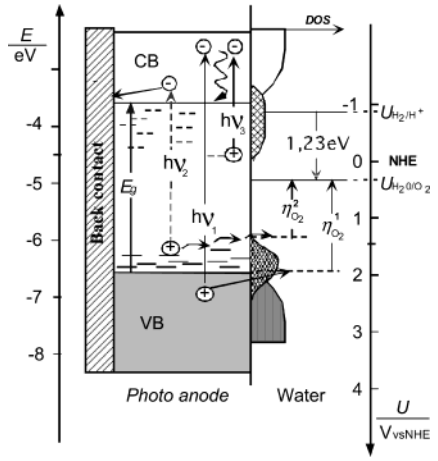

Figure 7. Illustration of the energetics and photoelectrochemical processes in $TiO_{2-x}N_x$. The vertical scales signify energy E in electronvolts and electrode potential U in V vs NHE, where NHE refers to the dihydrogen electrode under standard conditions. The positions of the standard electrode potential for dihydrogen $U(H_2/H^+)$ and dioxygen $U(H_2O/O_2)$ at standard conditions are given. The band gap energy of TiO_2 is indicated by E_g. The density of states (DOS) is *schematically* depicted for the valence band (VB; gray rectangle) and for the conduction band (CB; white rectangle). Lower hatched area shows the distribution of nitrogen-induced states in the vicinity of the VB (cf. ref 8), and upper hatched area shows the distribution of nitrogen-induced states below the CB as discussed in detail in the present work. $h\nu_1$ and $h\nu_2$ are photon energies in the ultraviolet and visible spectral ranges, respectively. The transport of photon-generated electrons (−) to the back contact and of photon-generated holes (+) to the electrode−electrolyte interface is shown. $h\nu_3$ is a photon energy in the infrared. These photons have energy enough to excite electrons from the states below the CB, introduce by nitrogen doping. $\eta(O_2)^1$ and $\eta(O_2)^2$ are the available over-potentials for water oxidation for holes from the VB and from the nitrogen-induced new states just above the VB, respectively.

options, we suggest that the former is the most important, at least at the low nitrogen doping levels of interest in the present work.

Our results are consistent with those of Irie et al.,[29] who found a difference in quantum efficiency between visible and UV light. They attributed their observation to excitations from an isolated narrow band above the valence band edge to the conduction band, rather than an excitation over a narrowed band gap. Lindgren et al.[10] also questioned the term "band gap narrowing" used by Asahi et al.[8] to describe the response to visible light. As pointed out by Irie et al.,[29] the calculations by Asahi et al.[8] were based on 6 at. % substitution of oxygen sites with nitrogen atoms, which is much higher than in the $TiO_{2-x}N_x$ material studied here. It is quite possible that the mobility of holes in the set of states just above the VB in $TiO_{2-x}N_x$ differs between large and small values of x.

IPCE$_\lambda$ Measurements. Incident photon-to-current conversion efficiency was studied with the same three-electrode setup as for the $j-V$ curves. Figures 8a and 8b show calculated spectral IPCE$_\lambda$ for an applied potential of 0.7 V. The dark current was negligible at this potential, and the electrolyte was again an aqueous solution of 0.1 M NaOH purged with nitrogen. As mentioned above, the IPCE$_\lambda$ measurements were carried out with irradiation through substrate−electrode interface (SE) as well as through electrolyte−electrode interface (EE). It can be seen in Figures 8a and 8b that the photoelectrochemical onset for the $TiO_{2-x}N_x$ electrode is located at a wavelength of ∼550 nm. The action spectrum fits the absorption spectrum well, which proves that that nitrogen-introduced states indeed are capable of separating light-induced holes and electrons. Data in the

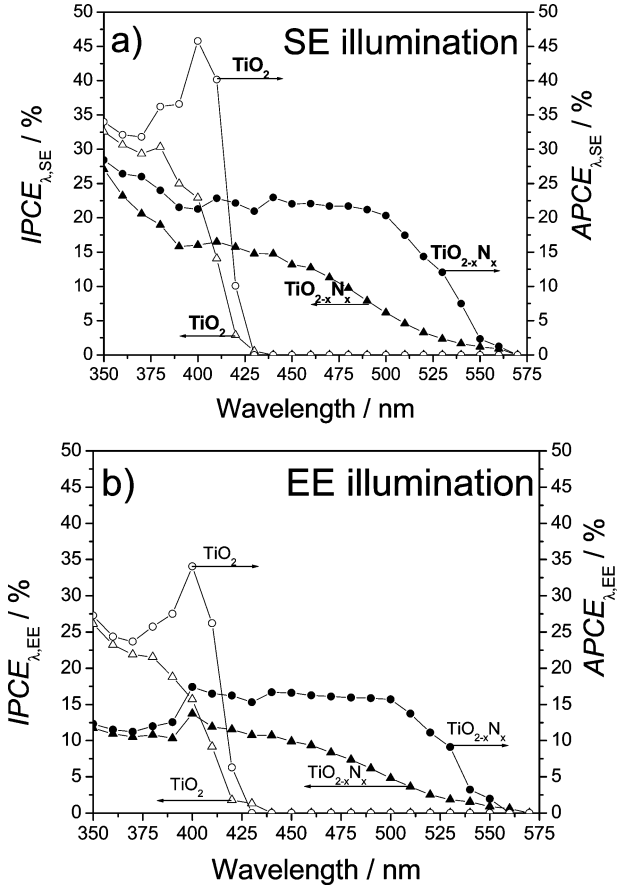

Figure 8. Spectral incident photon-to-current efficiency (IPCE$_\lambda$) and absorbed photon-to-current efficency (APCE$_\lambda$) of sputter-deposited $TiO_{2-x}N_x$ and TiO_2 films in 0.1 M NaOH at 0.7 V vs Ag/AgCl, as recorded for illumination from the substrate/electrolyte (SE) interface (a) and the electrolyte/electrolyte (EE) interface (b).

action spectra also show that illumination through the SE interface is more efficient than through the EE interface. This was observed for nitrogen-doped as well as for undoped TiO_2. Such a behavior is typical of nanoporous films, in which the charge carriers produced in the vicinity of the back contact are collected more efficiently;[30] it is contrary to the case of compact polycrystalline thin film electrodes.[22] For undoped TiO_2 there is a very small photoresponse in the $420 < \lambda < 550$ nm range, which likely can be ascribed to excitations to and from impurity states in the band gap. It is also interesting to notice that the photoresponse for undoped TiO_2 is higher than for nitrogen-doped TiO_2 in the UV region. This indicates that the nitrogen-doping-introduced band gap states, apart from increasing the photoresponse in the visible region, also contribute to recombination when the electrode is illuminated in the UV region.

Figure 8a shows that the APCE$_\lambda$ (see Section II for a definition) rises, beginning at 550 nm, up to a plateau value around 20% for $400 < \lambda < 500$ nm. This means that only twenty electrons per a hundred absorbed photons in the visible range contribute to the current in the outer circuit for $TiO_{2-x}N_x$.

Prospects for the Future. Despite the high rate of recombination in $TiO_{2-x}N_x$, a photocurrent of more than 0.2 mA per cm^{-2} was accomplished at a moderate bias of 0.55 V, with an electrode thickness far from being optimized (cf. Figure 6). The light source was a sulfur lamp emitting visible light and only a very minor fraction UV. The light intensity corresponded to approximately one sun. The photocurrent for undoped TiO_2 was negligible under the same conditions, a fact that may make nitrogen-doped TiO_2 an interesting material for photoelectro-

chemical applications. It has been shown theoretically that $TiO_{2-x}N_x$, with a spectral onset of photocurrent at around 550 nm, should be capable of converting solar light and electrical energy to chemical energy with an overall efficiency of 11%,[28] provided that no bias is needed. The question then is how efficient $TiO_{2-x}N_x$ can be as a thin film electrode.

At the present development stage for $TiO_{2-x}N_x$, slow transport of holes in a set of band gap states above the VB—together with electron trapping in states below the CB, enhancing the probability for recombination—limit the photoelectrochemical performance of the material both as a water-splitting electrode and as a photoanode in a solar cell for generation of electricity. The far from optimized thicknesses of the films, used in the present work, also contribute to the moderate performance of the nitrogen-doped electrodes. While the thickness issue can be remedied easily, the slow hole transport and the trapping states may be obstacles that are harder to overcome if they are an intrinsic property of nitrogen-doped TiO_2. The calculated density of states (DOS) by Asahi et al.[8] does not indicate that nitrogen doping causes any subband gap states below the conduction band edge. Assuming these calculations using full potential linearized augmented plane wave (FLAPW) formalism are correct, the states we observe below the conduction band edge may therefore equally well be ascribed to surface states, interstitial N atoms, or poor crystallinity of our material. If so, the material should be possible to improve by optimizing the preparation procedure.

IV. Summary

This work reported the photoelectrochemical behavior of nitrogen-doped TiO_2 in aqueous electrolyte. Nitrogen-doped thin films of mainly rutile TiO_2 were successfully prepared by reactive DC magnetron sputtering. Cross-sectional electron microscope images indicated a highly porous parallel penniform microstructure of $TiO_{2-x}N_x$. Action spectra, which corresponded well with optical data, showed a photoelectrochemical onset for $TiO_{2-x}N_x$ at a wavelength around 550 nm. Accordingly, the nitrogen-doped electrodes displayed a considerable increase in their photocurrent under visible light irradiation, compared to the case of undoped TiO_2. It was conclusively shown that dioxygen was generated photoelectrochemically by the $TiO_{2-x}N_x$ electrodes under steady-state illumination with visible light at anodic potentials exceeding −0.50 V vs Ag/AgCl (approximately −0.30 V vs NHE).

Compared to the case of TiO_2 electrodes, the onset potential of photocurrent for $TiO_{2-x}N_x$ was shifted anodically (by ∼0.8 V) when the electrode was scanned from positive toward negative potentials, while for anodic scans U_{on} remained approximately unchanged when compared to undoped TiO_2. It was further found that photostationary conditions led to an anodic shift of U_{on} to about −0.5 V, i.e., to a position between the U_{on} for the anodic and cathodic scan. The shift was ascribed to heavy recombination caused by a set of states in a broad regime below the conduction band. Interestingly, these states could be turned into long-lived electron traps when the electrode was illuminated at anodic potentials. The electron trap states were generated by UV, visible, and IR light (for $\lambda > 730$ nm). These electron traps could be monitored during cathodic scans as a "capacitive" rather than a faradic current. Thus it was shown that, apart from introducing an isolated band above the valence band edge,[10] nitrogen doping also introduced a *new* set of states positioned energetically in an 1.3 eV broad range just below the conduction band edge. These states may be intrinsic of the $TiO_{2-x}N_x$ material but may equally well be ascribed to surface states, interstitial N atoms, or poor crystallinity of our material. If so, the material should be possible to improve by optimizing the preparation procedure.

It was also noticed that the onset potential shifted differently depending on whether UV or visible light irradiation was used. The latter was explained by a lower mobility of the holes in the isolated nitrogen-created band above the VB edge[10] than of the mobility of the holes in the CB. Thus visible light excitation was followed by a higher loss of charge carriers due to recombination. Accordingly, the onset potential was shifted more anodically than under UV irradiation.

The high density of electron trapping states, leading to the observed massive recombination of charge carriers and producing a substantial anodic shift of U_{on}, seems to be an intrinsic property of the nitrogen-doped TiO_2. It is bound to the presence of nitrogen in the lattice and/or at the interface. If the recombination states mainly are at the surface, it is conceivable that the loss of photocurrent can be reduced by a posttreatment of the interface, and annealing of the $TiO_{2-x}N_x$ thin films may then help to reduce the density of recombination due to pathways other than those related to the nitrogen doping. Increasing the doping density should improve the mobility of the hole at will; on the other hand most probably it would also enhance the electron−hole recombination. Arguments of this kind could explain the pronounced optimum in the nitrogen content for giving the best photoresponse, as seen in earlier studies.[10] Currently we are working on fabricating thicker photoactive $TiO_{2-x}N_x$ films, for which an alternative thin film fabrication route will be considered. It starts with a nitrogen-doped TiO_2 powder,[29] which will be deposited by sol−gel methods and then sintered or pressed[31] onto the conducting glass.

Acknowledgment. The Swedish National Energy Agency supported this work. We are grateful to Professor H. Tributsch and Dr. K. Ellmer at the Hahn Meitner Institute, Berlin, Germany, for their help and discussions.

References and Notes

(1) Bak, T.; Nowotny, J.; Rekas, M.; Sorrell, C. C. *Int. J. Hydrogen Energy* **2002**, *27*, 991−1022.
(2) Fujishima, A.; Honda, K. *Nature* **1972**, *238*, 37.
(3) Grätzel, M. *Nature* **2001**, *414*, 338−344.
(4) Mills, A.; Le Hunte, S. *J. Photochem. Photobiol. A: Chemistry* **1997**, *108*, 1−35.
(5) Fujishima, A.; Rao, T. N.; Tryk, D. A. *J. Photochem. Photobiol. C: Photochemistry Reviews* **2000**, *1*, 1−21.
(6) O'Regan, B.; Grätzel, M. *Nature* **1991**, *353*, 737−740.
(7) Sato, S. *Chem. Phys. Lett.* **1986**, *123* (1, 2), 126−128.
(8) Asahi, R.; Morikawa, T.; Ohwaki, T.; Aoki, K.; Taga, Y. *Science* **2001**, *293*, 269−271.
(9) Morikawa, T.; Asahi, R.; Ohwaki, T.; Aoki, K.; Taga, Y. *Jpn. J. Appl. Phys.* **2001**, *40*, L561−L563.
(10) Lindgren, T.; Mwabora, J. M.; Avendaño Soto, E. D.; Jonsson, J.; Hoel, A.; Granqvist, C.-G.; Lindquist, S.-E. *J. Phys. Chem. B* **2003**, *107* (24), 5709−5716.
(11) Sakthivel, S.; Kisch, H. *ChemPhysChem* **2003,** *4*, 487−490.
(12) Grätzel, M. *Cattech* **1999**, *3*(1), 4−17.
(13) Khan, S. U. M.; Al-Shahry, M.; Ingler, W. B. J. *Science* **2002**, *297*, 2243−2245.
(14) Umebayashi, T.; Yamaki, T.; Itoh, H.; Asai, K. *Appl. Phys. Lett.* **2002,** *81* (3), 454−456.
(15) Umebayashi, T.; Yamaki, T.; Tanaka, S.; Asai, K. *Chem. Lett.* **2003**, *32* (4), 330−331.
(16) Nukumizu, K.; Nunoshige, J.; Takata, T.; Kondo, J. N.; Hara, M.; Kobayashi, H.; Domen, K. *Chem. Lett.* **2003**, *32* (2), 196−197.
(17) Rodríguez, J.; Gómez, M.; Lu, J.; Olsson, E. *Adv. Mater.* **2000**, *12* (5), 341−343.
(18) Gómez, M.; Rodríguez, J.; Lindquist, S.-E.; Granqvist, C.-G. *Thin Solid Films* **1999**, *342*, 148−152.
(19) Mwabora, J. M.; Lindgren, T.; Avendaño, E.; Jaramillo, T. F.; Lu, J.; Lindquist S.-E.; Granqvist, C.-G. *J. Phys. Chem. B*, submitted.

(20) Gómez, M. M.; Lu, J.; Solis, J. L.; Olsson, E.; Hagfeldt, A; Granqvist, C.-G. *J. Phys. Chem. B* **2000**, *104*, 8712−8718.

(21) Rodríguez, J.; Gómez, M.; Lu, J.; Olsson, E.; Granqvist, C.-G. *Adv. Mater.* **2000**, *12* (5), 341−343.

(22) Lindquist, S.-E.; Finnström, B.; Tegnér, L. *J. Electrochem. Soc.: Electrochemical Science and Technology* **1983**, *130* (2), 351−358.

(23) Rensmo, H.; Lindström, H.; Södergren, S.; Willstedt, A.-K.; Solbrand, A.; Hagfeldt, A.; Lindquist, S.-E. *J. Electrochem. Soc.* **1996**, *143* (10), 3173−3178.

(24) Sato, N. *Electrochemistry at Metal and Semiconductor Electrodes*; Amsterdam: Elsevier Science B. V., 1998; pp 325−371.

(25) Carey, J. H.; Oliver, B. G. *Nature* **1976**, *259*, 554−556.

(26) Gerischer, H. *J. Electrochem. Soc.* **1966**, *113*, 1174.

(27) Lindquist, S.-E.; Vidarsson, H. *J. Mol. Catal.* **1986**, *38*, 131.

(28) Lindgren, T.; Romualdo Torres, G.; Lu, J.; Granqvist, C.-G.; Lindquist, S.-E. *Sol. Energy Mater. Sol. Cells*, submitted.

(29) Irie, H.; Watanabe, Y.; Hashimoto, K. *J. Phys. Chem. B* **2003**, *107* (23), 5483−5486.

(30) Hagfeldt, A.; Björksten, U.; Lindquist, S.-E. *Sol. Energy Mater. Sol. Cells* **1992**, *27*, 293−304.

(31) Lindström, H.; Magnusson, E.; Holmberg, A.; Södergren, S.; Lindquist, S.-E.; Hagfeldt, A. *Sol. Energy Mater. Sol. Cells* **2002**, *73*, 91−101.